Proceedings of the 20th International Conference on Soil Mechanics and Geotechnical Engineering– Rahman and Jaksa (Eds)

Mechanical properties of cement under supercritical carbonation

Propriétés mécaniques du ciment sous carbonatation supercritiques

Diego Manzanal
E.T.S.I. de Caminos, Canales y Puertos, Universidad Politécnica de Madrid, Spain.

Juan Cruz Barría, Sandra Orlandi, Ricardo Guerreiro
Laboratorio de Investigación de Suelos, Hormigones y Asfaltos, Universidad Nacional de la Patagonia San Juan Bosco, Argentina

Siavash Ghabezloo & Jean-Michel Pereira
Navier, École des Ponts, Univ. Gustave Eiffel, CNRS, France

ABSTRACT: Geo-storage of carbon dioxide has been gaining importance over the years through the growing interest of people and governments in reducing greenhouse gas emissions. It has already been proven in the field, especially through drilling methods already known in the oil industry, making this alternative possible. The reservoir well consists of a steel casing, which is externally coated with cement. Initially, the cement is capable of sustaining external stresses. However, the well will be exposed for many years to carbon dioxide in a supercritical state. The carbonation leads to the dissolution of the cement main components and the degradation of its cementitious matrix, resulting in the creation of leakage pathways through cement and in the loss of stability of the well. This work aims to study the long-term variations of the mechanical parameters of cement when it carbonates under supercritical conditions. We carbonated cement samples at high temperature and high pressure, thus representing the reservoir conditions. The mechanical properties were obtained throughout the use of high-pressure triaxial equipment for rocks. The parameters obtained were used to calibrate a coupled chemical-hydro-mechanical model implemented in a finite element code.

RÉSUMÉ : Le géo-stockage du dioxyde de carbone a gagné en importance au fil des ans en raison de l'intérêt croissant des personnes et des gouvernements pour la réduction de la des émissions de gaz à effet de serre. Il a déjà fait ses preuves sur le terrain, notamment grâce à des méthodes de forage déjà connues dans l'industrie pétrolière, ce qui rend cette alternative possible. Le puits-réservoir est constitué d'un tubage en acier, qui est recouvert extérieurement de ciment. Initialement, le ciment est capable de supporter les contraintes externes. Cependant, le puits sera exposé pendant de nombreuses années au dioxyde de carbone à l'état supercritique. La carbonatation conduit à la lixiviation des principaux composants du ciment et à la dégradation de sa matrice cimentaire, ce qui peut entraîner la création de voies de fuite à travers le ciment et la perte de stabilité du puits. Le but de ce travail est d'étudier les variations à long terme des paramètres mécaniques du ciment lorsqu'il se carbonate dans des conditions supercritiques. Des échantillons de ciment ont été carbonatés à haute température et haute pression, représentant ainsi les conditions du réservoir. Les propriétés mécaniques ont été obtenues grâce à l'utilisation d'un équipement triaxial à haute pression pour les roches. Les paramètres obtenus ont été utilisés pour calibrer un modèle couplé chimique-hydro-mécanique implémenté dans un code aux éléments finis.

KEYWORDS: CO_2 geological storage – Cement paste – Supercritical carbonation – Triaxial tests – Numerical simulations

1 INTRODUCTION.

The increased demand for energy from economic growth in the world also leads to higher CO_2 emissions (Aminu et al., 2017). One way to reduce the atmospheric pollution generated by these emissions is to divert the flow of CO_2 into geological reservoirs (Chen and Xu, 2010), storing a large amount of this gas (Michael et al., 2010).

The geological reservoirs to be considered are coal beads, deep aquifer reservoirs, or abandoned oil reservoirs. It must be ensured that the upper caprock of the reservoir is sufficiently impermeable and resistant so that once the CO_2 is injected, it does not percolate through the upper formations.

The way to inject CO_2 into a geological reservoir is to drill to the desired depth and inject it. However, this task requires the injection well to be stable and safe. A steel pipe is placed perfectly centered in the borehole, and then a cement slurry is injected to protect it from corrosion and seal the well. Cement requires a high pH to remain in chemical equilibrium, while CO_2-bearing geological reservoirs impose an acidic environment that is corrosive to cement.

The carbonation process is characterized by the chemical reactions between the CO_2 bearing-fluids with the hydrated cement products, mainly calcium hydroxide (CH) in Eq. 1 and calcium silicate hydrate (C-S-H) in Eq. 2, to produce calcium carbonates ($CaCO_3$ or CC) and amorphous silica (AmSi):

$$\mathrm{CH} + \mathrm{CO_2} \rightarrow \mathrm{CaCO_3} + \mathrm{H_2O} \quad (1)$$

$$\mathrm{C-S-H} + 1.7\ \mathrm{CO_2} \rightarrow 1.7\ \mathrm{CaCO_3} + \mathrm{AmSi} \quad (2)$$

These reactions change the cement matrix generating discontinuities within the material and modifying the pore structure. One of the main problems is the total dissolution of cement hydrates, leaving amorphous silica and calcium carbonates. Also, calcium carbonates may be re-dissolve if pH conditions permit (Zhang and Bachu, 2011) or could be washed away by a flow corresponding, for example, to the constant injection of CO_2.

In turn, the high pressure and high temperature in these reservoirs can cause CO_2 to be in a supercritical state, above 32°C and 7 MPa. At this point, the CO_2 becomes very dense and with low viscosity, further enhancing storage capacity but also the carbonation of the cement.

This work aims to study the variation of the mechanical properties of cement once it is subjected to carbonation at a pressure of 20 MPa and 90°C of temperature. This is carried out

through isotropic triaxial tests to determine the compressibility moduli and with deviatoric tests in the elastic zone to determine Young's modulus and Poisson's ratio.

A numerical simulation of carbonation is also presented using the finite element method with a chemo-hydro-mechanical coupled model. The reaction advance and the porosity variation through time were determined.

2 MATERIALS AND METHODS

Cement samples were prepared according to the American Petroleum Institute Standard 10A (API Specification 10A, 2019). Samples were prepared and poured in cylindrical molds for 24 h and then removed from the mold. Later, they were cured for 28 days in lime-saturated water at 20°C (Barría et al., 2020a). Once removed from the batch, they were cut to obtain cylindrical samples of 38x76 mm.

2.1 *Carbonation*

Carbonation was performed in a titanium cell at 20 MPa and 90°C in static conditions. The samples were allowed to carbonate in wet supercritical CO_2 for 30 days, as presented in previous works (Barría et al., 2020a). Figure 1 shows the carbonation cell used.

Figure 1. Carbonation cell

2.2 *Triaxial tests*

Triaxial tests were performed on cement samples to determine the mechanical properties at different confining conditions, simulating underground conditions.

Cylindrical cement samples of 38 mm in diameter and 76 mm long were placed inside a neoprene membrane. Two linear variable differential transformers (LVDT) were positioned in the axial direction and four in the radial direction touching a thin aluminum sheet glued to the four radial pierced holes in the membrane.

Porous stones were placed on the top and bottom of the samples to allow a homogeneous pore pressure distribution. Pore pressure, confining pressure, and deviatoric loading were measured by electronic transducers and controlled by software linked to hydraulic pumps.

The tests performed were:

- Undrained isotropic test
- Drained isotropic test
- Deviatoric test

The isotropic tests were performed with initial confining values ranging from 5 to 30 MPa. The isotropic load increases to a certain value and then unloads to the initial value. The bulk modulus of the sample is measured from the load-unload curve.

In the undrained isotropic test, the pore pressure exit valve is closed, preventing mass exchange. In this case, the increase in pore pressure within the sample is measured through pressure sensors. Reversely, for the drained isotropic test, the exit valve is open to let the water evacuate the sample.

The deviatoric test was performed under undrained conditions. The variation in pore pressure and deformation of the sample was measured.

The parameters obtained during triaxial tests were undrained bulk modulus (Ku), Skempton coefficient (B), drained bulk modulus (Kd), Young's modulus (E_u) and Poisson coefficient (ν_u) in undrained conditions.

3 RESULTS

Figure 2 shows the samples affected after 30 days of carbonation. Some of the samples were damaged and broken during the tests, probably due to depressurization.

Density increases from 1.99 to 2.02 g/cm^3 with a mass uptake average of 2.7 g per sample. This is a result of the higher density of carbonates compared to CH, and due to the higher amount of CC produced in the reaction of Eq. 1 with a CC/C-S-H ratio of 1.7.

Figure 2. Samples after 30 days of supercritical carbonation at 20MPa and 90°C.

The isotropic tests are shown in Figure 3, where the isotropic load increase is plotted as a function of the volumetric deformations. The bulk modulus corresponds to the slopes of every curve.

As expected, before carbonation the undrained slopes are steeper than the drained slopes. This is because drained samples allow greater deformation by allowing water inside them to escape, making them more compressible.

The Skempton coefficient can be measured from pore pressure measurements on the sample during the isotropic test. This coefficient corresponds to the slope of the pressure increase

curve as a function of the applied isotropic load (Skempton, 1954). This coefficient is influenced by the degree of saturation of the sample, if the sample is not completely saturated, the measured Skempton coefficient will be lower compared to that of the saturated sample.

A small increment in the bulk modulus is observed when the initial confining pressure is higher. This is due to the fact that when applying a higher initial confining load, the pore structure is reduced, allowing smaller deformations when an external load is applied.

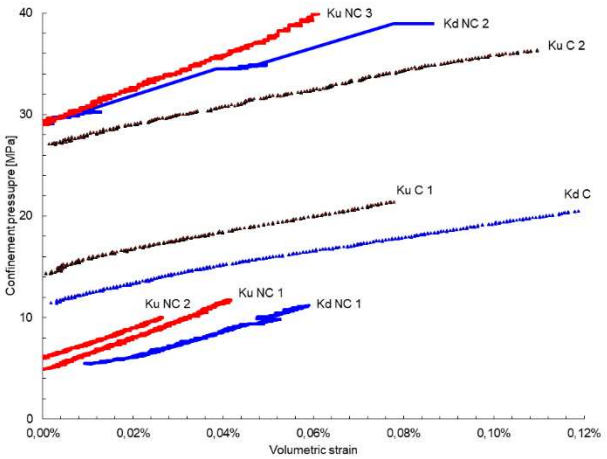

Figure 3. Isotropic drained (Kd) and undrained (Ku) measurements of triaxial tests on carbonated (C) and non-carbonated (NC) samples. The slopes correspond to the bulk modulus.

Figure 4 shows the bulk modulus in function of the initial confining pressure during the isotropic test. The values of drained and undrained bulk modulus are in accordance with those in the literature (Ghabezloo et al., 2008; Samudio, 2018)

Once the samples are carbonated, the slopes are lower, indicating that more volumetric deformation is produced when an isotropic load is applied.

The edge of the sample in contact with CO_2 undergoes dissolution of cementitious material and precipitation of $CaCO_3$. This generates a degraded region in which 3 zones can be observed (Kutchko et al., 2008): the leaching zone, the precipitation zone, and the re-dissolution zone. The latter zone, which is in direct contact with the fluid in the supercritical state, is the most affected. This is where carbonates dissolve in the fluid and porosity increases (Bagheri et al., 2019). This zone can vary its thickness depending on the curing and carbonation condition imposed to cement (Jeong et al., 2018; Xu et al., 2019).

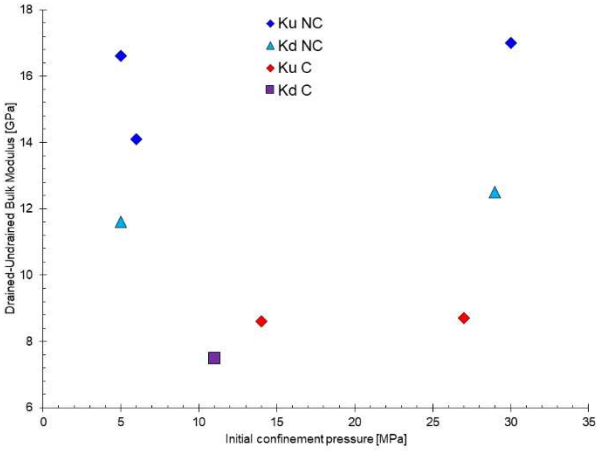

Figure 4. Bulk modulus of drained (Kd) and undrained (Ku) tests on carbonated (C) and non-carbonated (NC) samples. Results are shown as function of the initial confining pressure of each test.

By applying an isotropic load to the carbonated cement, this outer zone, with a lower Ca/Si ratio due to the re-dissolution of the $CaCO_3$, is more susceptible to deformation than before carbonation. As the total volumetric strain is higher after each load increment, the final slope of the curves in Figure 3 is lower, thus corresponding to a reduced bulk modulus of the sample.

The averages values obtained from all the isotropic tests are shown in Table 1. Carbonation reduces drained and undrained bulk moduli by up to 40%, while the Skempton coefficient does not vary significantly.

Table 1. Averages bulk modulus values obtained from isotropic tests at different confining pressures

Measured parameter	*Non-carbonated*	*Carbonated*
Ku [GPa]	15.30	8.60
Skempton coef.	0.32	0.34
Kd [GPa]	12.00	7.50

The Young's modulus and Poisson ratio are taken from the elastic zone of Figure 5. Both parameters are taken from the same range of load application, between 4 and 15 MPa of deviatoric stress. Table 2 shows the results of Young's modulus and Poisson ratio for non-carbonated and carbonated samples.

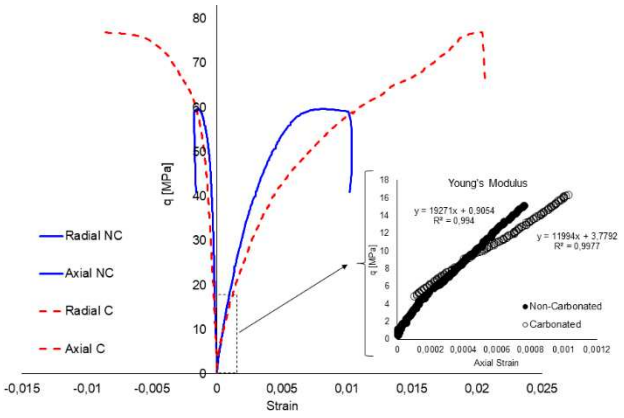

Figure 5. Deviatoric test on non-carbonated (NC) and carbonated (C) samples.

The elastic relationship between the bulk modulus, Young's Modulus, and Poisson's ratio can be obtained by the following equation:

$$\nu_u = \frac{3K_u - E_u}{6K_u} \quad (3)$$

With an undrained bulk modulus of 15,30 GPa and Young's modulus of 19.2 GPa, we obtain a Poisson ratio of 0.29. The difference with the measured value is probably due to the accuracy of the data acquisition. Averaging the experimental (0.23) and theoretical value (0.29), we can determine a Poisson ratio of 0.26.

Table 2. Elastic parameters obtained from deviatoric tests for unconfined conditions

Measured parameter	*Non-carbonated*	*Carbonated*
E_u [GPa]	19.2	12.00
μ_u	0.23	0.19

The carbonation front generates the dissolution of the cementitious material at a certain distance from the edge and also a redissolution of the carbonates that precipitate near the edge.

Since the material is no longer isotropic, the elastic relationship of Eq. 3 is not valid. Therefore, numerical approximations must be used to determine the properties in the affected zone.

4 NUMERICAL RESULTS

In this section, the experimental tests are simulated with a chemo-poromechanical coupled model (Vallin et al., 2013) implemented in a finite element code BIL 2.3.0 (Dangla and Bonnard, 2017).

The model can simulate the carbonation advance in 1D or 2D materials. It contains the balance equations of the continuum mechanics based on conservation of mass, momentum, and energy (Vallin, 2014).

The pore structure of the materials is considered as fully saturated, and the CO_2 is a dissolved species within the fluid. As cement starts to carbonate, its porosity suffers several variations. The solid phases of CH and C-S-H are dissolved, and CC precipitates in the pores.

The model considers an elastic isotropic porous material for the infinitesimal representative volume element. The poroelastic equations balance in isothermal conditions are the following:

$$\boldsymbol{\sigma} - \boldsymbol{\sigma_0} = \left(\mathrm{K} - \frac{2}{3}\mathrm{G}\right)(\varepsilon - \varepsilon_0)\mathbf{1} + 2\mathrm{G}(\boldsymbol{\varepsilon} - \boldsymbol{\varepsilon_0}) - \sum_{\mathrm{k=F,C}} \mathrm{b_k}(\mathrm{p_k} - \mathrm{p_{k,0}})\mathbf{1} \quad (3)$$

$$\varphi_J - \varphi_{J,0} = b_J(\varepsilon - \varepsilon_0) + \sum_{k=F,C} \frac{p_k - p_{k,0}}{N_{JK}}; J = F, C \quad (4)$$

Where:

$\boldsymbol{\sigma}$: is the stress tensor

$\boldsymbol{\varepsilon}$: is the infinitesimal strain tensor

ε: is the volumetric strain. ($\mathrm{tr}(\boldsymbol{\varepsilon})$)

K, G: are the bulk and shear moduli in drained conditions

φ_J: is deformation of porous volume occupied by the phase J

b_J: is the generalized Biot coefficient

N_{JK}: is the generalized poroelastic coupling moduli (Coussy, 2010).

The mass conservation is applied to the fluid and to the molar amount of CO_2

$$\left(\frac{\rho_f \phi_f}{K_f} + \frac{\rho_f}{N_{FF}}\right)\frac{\partial p_f}{\partial t} + \rho_f b\, div\left(\frac{\partial \boldsymbol{u}}{\partial t}\right) + \rho_f \sum_{R_i} Y_{Ri} \frac{\partial \xi_{Ri}}{\partial t} - div\left(\rho_f \frac{\kappa}{\eta} grad\, \rho_f\right) = 0 \quad (5)$$

$$\frac{\partial(\phi_f c_{CO_2})}{\partial t} + \sum_{R_i} a_{Ri} \frac{\partial \xi_{Ri}}{\partial t} - div\left(d_{eff}\, \boldsymbol{grad}\, c_{CO_2} + c_{CO_2} \frac{\kappa}{\eta} \boldsymbol{grad}\, \rho_f\right) = 0 \quad (6)$$

Where:

ρ_f is the density of the fluid.

ϕ_f is the fluid porosity.

K_f is the bulk modulus of the fluid.

p_f is the fluid pressure.

a_{Ri} is the stoichiometric coefficient of the reaction Ri

c_{CO_2} is the CO_2 concentration in fluid.

η is the dynamic viscosity of the fluid phase.

Y_{Ri} is a variable that depends on the molar volumes of reactive species

$\boldsymbol{u}$ is the skeleton displacement vector.

ξ_{Ri} is the reaction advance depending on κ and d_{eff}, which are the permeability and diffusion coefficients.

The carbonation progress is ruled by the diffusion and permeability transport phenomena (Ghabezloo et al., 2009; Mainguy, 1999).

The samples carbonated in the cell are submitted to a pressure of 20 MPa and a temperature of 90°C. As the code is not thermally coupled, the fluid and gas conditions are set for a constant temperature of 90°C.

To simulate the carbonation advance in these samples, a 2D rectangular shape model was used. The rectangular shape consisted of one-quarter of a sample (19 mm-radius by 38 mm-height) using a mesh of 22x11 elements (Figure 6). The bottom horizontal contour has restricted movements in the Y direction, while the left vertical contour has restricted movements in the X direction. The top and right-hand contours are subjected to carbonation.

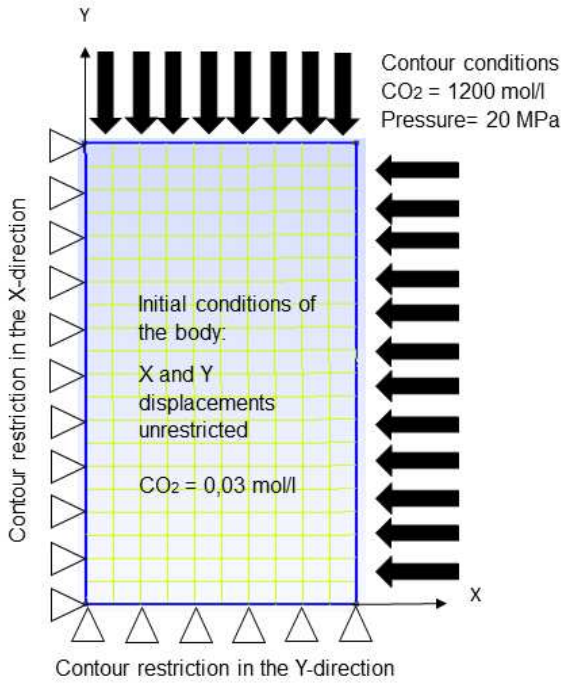

Figure 6. Carbonation model simulated with finite elements.

In the experimental results, the carbonation front advances between 4 and 6 millimeters (Barría et al., 2020b). The small penetration compared to other authors (Fabbri et al., 2009; Kutchko et al., 2007) is due to the long curing period for the samples of this work. This reduces porosity and slows down the diffusion of CO_2 into the sample (Mainguy, 1999). Figure 7 shows the level of CO_2 concentration in one quadrant of the sample, which roughly indicates the progress of the chemical reactions.

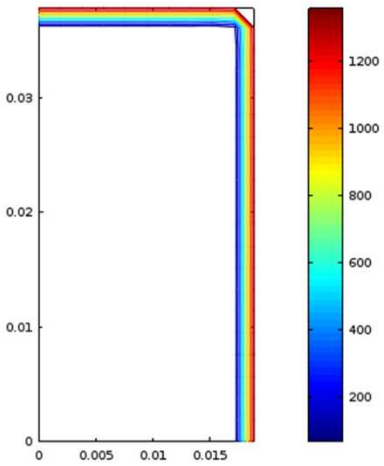

Figure 7. Carbonation advance in the sample after 30 days of carbonation.

Once precipitation started, the precipitation could either present a clogging effect over the porous media or simply dissolve the cementitious compounds (Brunet et al., 2013). The dissolution can occur in samples with high porosity and low CH amount. The clogging effect is more likely to occur in samples with low porosity and high portlandite content.

The initial capillary porosity of 20% (Barría et al., 2020b) and the high level of portlandite (Barría et al., 2021) in these samples generate the conditions for the porosity to decrease significantly over time, as can be seen in Figure 8. The porosity of the edges is reduced from 20% to 13.5 %.

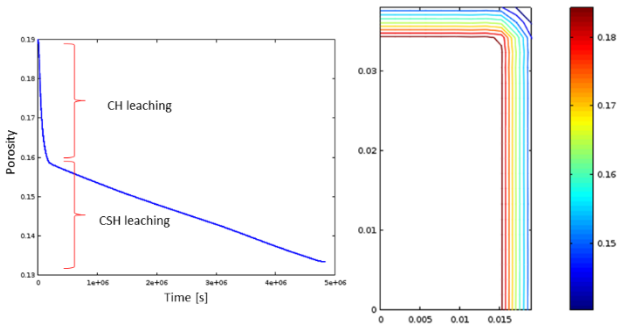

Figure 8. (a) Porosity development overtime for a point near the outer rim. (b) Porosity profile of the samples carbonated after 30 days in the supercritical CO_2

The first carbonation reaction rapidly depletes the CH content of the sample. This reduces the pH level, and the C-S-H carbonation starts when this level is below 10.5 (Alexander et al., 2013). C-S-H decalcification extends to 30 days of carbonation. This reduces the Ca/Si ratio in the C-S-H structure and precipitates more $CaCO_3$ inside the pores slowing down further carbonation.

5 CONCLUSIONS

Preliminary results were obtained from triaxial tests on carbonated samples after being carbonated under supercritical CO_2 conditions at 20 MPa and 90°C for 30 days.

Isotropic drained and undrained tests were carried out to obtain the drained and undrained moduli of carbonated cement samples. Later, a deviatoric loading was applied to determine Young's modulus and Poisson ratio.

These results were taken to calibrate a chemo-poromechanical model implemented in a finite element code. The carbonation reactions in the carbonation cell were simulated.

The values of the bulk moduli and Skempton coefficient before carbonation are following those found in the literature.

Carbonation generates a degraded zone at the edges of the samples. When an isotropic load is applied, the sample is more compressible, so the bulks moduli of the samples decreased. In turn, when a deviatoric load is applied, the undrained Young's modulus is reduced.

The numerical analysis performed roughly simulates the carbonation advance and how porosity varies with time, indicating that the samples show a clogging effect as carbonation advances.

Further studies with triaxial loading are needed to precisely determine the poromechanical behavior of carbonated cement samples with different curing and carbonation conditions.

6 REFERENCES

Aminu, M.D., Ali, S., Rochelle, C.A., Manovic, V., 2017. A review of developments in carbon dioxide storage. Appl. Energy 0–1. https://doi.org/10.1016/j.apenergy.2017.09.015

API Specification 10A, 2019. Specification for Cements and Materials for Well Cementing, Twenty-Fif. ed, American Petroleum Institute. Northwest Washington, DC.

Bagheri, M., Shariatipour, S.M., Ganjian, E., 2019. Prediction of the lifespan of cement at a specific depth based on the coupling of geomechanical and geochemical processes for CO2 storage. Int. J. Greenh. Gas Control 86, 43–65. https://doi.org/10.1016/j.ijggc.2019.04.016

Barría, J.C., Manzanal, D., Pereira, J.M., Ghabezloo, S., 2020a. CO2 geological storage: Microstructure and mechanical behavior of cement modified with a biopolymer after carbonation. E3S Web Conf. 205. https://doi.org/10.1051/e3sconf/202020502007

Barría, J.C., Manzanal, D.G., Martín, C.M., Piqué, T., Pereira, J.M., 2020b. Cement-rock interface subjected to SCCO2, in: Rock Mechanics for Natural Resources and Infrastructure Development-Proceedings of the 14th International Congress on Rock Mechanics and Rock Engineering, ISRM 2019. pp. 3196–3203.

Barría, J.C., Vázquez, A., Pereira, J.M., Manzanal, D., 2021. Effect of bacterial nanocellulose on the fresh and hardened states of oil well cement. J. Pet. Sci. Eng. 199. https://doi.org/10.1016/j.petrol.2020.108259

Brunet, J.P.L., Li, L., Karpyn, Z.T., Kutchko, B.G., Strazisar, B., Bromhal, G., 2013. Dynamic evolution of cement composition and transport properties under conditions relevant to geological carbon sequestration. Energy and Fuels 27, 4208–4220. https://doi.org/10.1021/ef302023v

Chen, W., Xu, R., 2010. Clean coal technology development in China. Energy Policy 38, 2123–2130. https://doi.org/10.1016/j.enpol.2009.06.003

Coussy, O., 2010. Mechanics and Physics of Porous Solids, Mechanics

and Physics of Porous Solids. https://doi.org/10.1002/9780470710388
Dangla, P., Bonnard, A., 2017. Ifsttar/bil: first version in github (Version v2.4). Zenodo. https://doi.org/10.5281/zenodo.1039729
Fabbri, A., Corvisier, J., Schubnel, A., Brunet, F., Goffé, B., Rimmele, G., Barlet-Gouédard, V., 2009. Effect of carbonation on the hydro-mechanical properties of Portland cements. Cem. Concr. Res. 39, 1156–1163. https://doi.org/10.1016/j.cemconres.2009.07.028
Ghabezloo, S., Sulem, J., Guédon, S., Martineau, F., Saint-Marc, J., 2008. Poromechanical behaviour of hardened cement paste under isotropic loading. Cem. Concr. Res. 38, 1424–1437. https://doi.org/10.1016/j.cemconres.2008.06.007
Ghabezloo, S., Sulem, J., Saint-Marc, J., 2009. Evaluation of a permeability-porosity relationship in a low-permeability creeping material using a single transient test. Int. J. Rock Mech. Min. Sci. 46, 761–768. https://doi.org/10.1016/j.ijrmms.2008.10.003
Jeong, Y.J., Youm, K.S., Yun, T.S., 2018. Effect of nano-silica and curing conditions on the reaction rate of class G well cement exposed to geological CO2-sequestration conditions. Cem. Concr. Res. 109, 208–216. https://doi.org/10.1016/j.cemconres.2018.05.001
Kutchko, B.G., Strazisar, B.R., Dzombak, D.A., Lowry, G. V, Thaulow, N., 2007. Degradation of Well Cement by CO2 under Geological Sequestration Conditions. Env. Sci Technol 41, 4787–4792. https://doi.org/10.1021/es062828c
Kutchko, B.G., Strazisar, B.R., Lowry, G.V., Dzombak, D. a., Thaulow, N., 2008. Rate of CO2 Attack on Hydrated Class H Well Cement under Geologic Sequestration Conditions. Environ. Sci. \& Technol. 42, 6237–6242. https://doi.org/10.1021/es800049r
Mainguy, M., 1999. modeles de diffusion non-lineaires en milieux poreux. Applications a la dissolution et au sechage des materiaux cimentaires.
Michael, K., Golab, A., Shulakova, V., Ennis-king, J., Allinson, G., Sharma, S., Aiken, T., 2010. Geological storage of CO 2 in saline aquifers — A review of the experience from existing storage operations. Int. J. Greenh. Gas Control 4, 659–667. https://doi.org/10.1016/j.ijggc.2009.12.011
Samudio, M., 2018. Modelling of an oil well cement paste from early age to hardened state : hydration kinetics and poromechanical behaviour To cite this version : Université Paris-Est.
Skempton, A.W., 1954. The pore-pressure coefficients a and b. Geotechnique 4, 143–147. https://doi.org/10.1680/geot.1954.4.4.143
Vallin, V., 2014. Modélisation chimio poromécanique du comportement des géomatériaux dans le contexte du stockage géologique du dioxyde de carbone : Application au puits d'injection. Université Paris-Est.
Vallin, V., Pereira, J.M., Fabbri, A., Wong, H., 2013. Numerical modelling of the hydro-chemo-mechanical behaviour of geomaterials in the context of CO 2 injection 3052–3069. https://doi.org/10.1002/nag
Xu, B., Yuan, B., Wang, Y., Zeng, S., Yang, Y., 2019. Nanosilica-latex reduction carbonation-induced degradation in cement of CO2 geological storage wells. J. Nat. Gas Sci. Eng. 65, 237–247. https://doi.org/10.1016/j.jngse.2019.03.013
Zhang, M., Bachu, S., 2011. Review of integrity of existing wells in relation to CO2 geological storage: What do we know? Int. J. Greenh. Gas Control 5, 826–840. https://doi.org/10.1016/j.ijggc.2010.11.006